Research Article

Journal of Geophysical Research: Oceans
DOI 10.1002/2018JC013949

Coherent circulation changes in the deep North Atlantic from 16°N and 26°N transport arrays

E. Frajka-Williams[1], M. Lankhorst[2], J. Koelling[2], and U. Send[2]

[1]Ocean and Earth Science, University of Southampton, Southampton, SO14 3ZH
[2]Scripps Institution of Oceanography, University of California San Diego, La Jolla, USA

Key Points:

- Coherent hydrographic changes are observed at 16°N and 26°N in western Atlantic.
- At both latitudes, reducing densities below 1000 m have resulted in intensified zonal shear since 2009/10.
- Opposing decadal trends of the MOC at the two latitudes result from geostrophic reference level choices.

Corresponding author: Eleanor Frajka-Williams, e.frajka-williams@soton.ac.uk

Received: Mar 03, 2018; Revised: Apr 09, 2018; Accepted: Apr 11, 2018

Abstract

The meridional overturning circulation (MOC) has been measured by boundary arrays in the Atlantic since 2000. Over the past decade of measurements, however, the reported tendencies in overturning circulation strength have differed between 16°N and 26°N. Here, we investigate these differences by diagnosing their origin in the observed hydrography, finding that both arrays show deep waters (below 1100 dbar) at the western boundary becoming fresher and less dense. The associated change in geopotential thickness is about 0.15 m^2s^{-2} between 2004–2009 and 2010–2014, with the shift occurring between 2009–2010 and earlier at 26°N than 16°N. In the absence of a similar density change on the east of the Atlantic, this mid-depth reduction in water density at the west would drive an increase in the shear between the upper and lower layers of North Atlantic Deep Water of about 2.6 Sv at 26°N and 3.9 Sv at 16°N. These transport anomalies result in an intensifying tendency in the MOC estimate at 16°N, but at 26°N, the method of correcting the geostrophic reference level results in an opposing (reducing) tendency of the MOC. The results indicate that both arrays are observing coherent, low frequency changes, but that there remain discrepancies in the methods of addressing the geostrophic reference level for boundary arrays measuring ocean circulation.

1 Introduction

The large-scale ocean circulation is often displayed in schematics with ribbons of red and blue indicating warm and cold transports at different depths [e.g., *Broecker*, 1991; *Black*, 2010]. These schematics capture several key aspects of the meridional overturning circulation (MOC): that it includes warm thermocline waters flowing northwards in the top 1000 m of the Atlantic and colder waters at depth moving generally southwards. The thermocline waters carry heat northwards, while the deep waters, recently formed through interaction with the atmosphere at the surface, store carbon and other properties at depth. Zonally-averaging this circulation across the Atlantic basin from east-to-west, the meridional flow (flow in the north-south direction) shows "overturning" with surface waters moving northwards, deepening, then returning southwards at depth [*Danabasoglu et al.*, 2014]. The strength of the overturning then refers to the total northward flow in the top ~1000 m of the Atlantic, which is equal and opposite to the southward flow below. This overturning is typically about 17–20 Sv [1 Sv = 1,000,000 m^3s^{-1}; *Lozier*, 2010, 2012; *Srokosz and Bryden*, 2015].

Schematics of overturning, while capturing some of the salient features, also connote a circulation that is simple and laminar, and when referred to as a "great conveyor" suggest a conveyor belt moving at similar speeds everywhere. While time-mean circulation shows a continuous northward flow across the tropics to mid-latitudes in the Atlantic, variations in the strength of overturning at different latitudes may not be simultaneous. A long simulation (1000 years) of the time-varying overturning circulation identified lower frequency fluctuations in the subpolar regions and interannual variations in subtropical regions [*Zhang*, 2010]. In particular, the subtropical transport magnitude exhibited variations of the same sign as those in the subpolar regions, but at some time delay. More realistic simulations investigating the coherence of the overturning find that across the subtropics, fluctuations are relatively coherent, meaning instantaneously correlated, on interannual timescales [$r > 0.6$ between 0–40°N; *Bingham et al.*, 2007]. Differences in the strength of overturning between latitudes may result in local convergences or divergences of heat [*Cunningham et al.*, 2013; *Kelly et al.*, 2014] which may in turn drive heat fluxes into or out of the atmosphere.

Moored estimates of the time-varying transports in the Atlantic show substantial interannual and sub-annual variability [*Frajka-Williams et al.*, 2016; *Send et al.*, 2011; *Toole et al.*, 2011]. However, efforts to link observations between distant individual latitudes have been stymied by phase differences between sub-annual variations of the MOC [*Elipot*

et al., 2014; *Mielke et al.*, 2013; *Dong et al.*, 2015]. *Mielke et al.* [2013] showed that the seasonal cycles of the non-Ekman component of the overturning were 180° out-of-phase between 26°N and 41°N, though the phasing of the observed seasonal cycle at 41°N did not agree with the modeled seasonal cycle. *Elipot et al.* [2014] also identified an out-of-phase relationship between the large-scale transport fluctuations at different latitudes but used only the western boundary density signals to compute transports. Some of these fluctuations in transport have been found to have a fixed relationship to two modes of wind stress variability over the Atlantic [*Elipot et al.*, 2017], with locations at 16°N and 26°N related to the first mode of variability, and the more northerly regions ($\sim$ 40°N) to the North Atlantic Oscillation pattern of wind forcing over a 3.6 year period between 2004 and 2009.

On longer (interannual-to-one-decade) timescales, where the overturning circulation may be expected to represent larger-scale basin-wide fluctuations in ocean circulation, the MOC at 26°N has reported a weakening trend over the period 2004–2012 [*Smeed et al.*, 2014]. Similarly, at 16°N, the reported transports showed a weakening MOC over 2000–2010, resulting primarily from density tendencies at the Mid-Atlantic Ridge [*Send et al.*, 2011]. We will show that over the overlapping period, the reported tendencies of the MOC strength at the two latitudes are opposing. Transports at both latitudes are monitored using a boundary mooring approach, where temperature and salinity profiles are measured continuously at western and eastern edges, spanning great swaths of the ocean. The method of calculating transports relies on the thermal wind relation between meridional shear in transports and zonal density gradients. However, thermal wind only determines the velocity shear relative to a level of no or known motion. The methods used to compute transports at the two latitudes differ in their application of a choice of reference level.

In this paper, we explore whether or not the MOC is coherent between 16°N and 26°N in the Atlantic, from observations. In section 2, the data and methods are described. In section 3, we discuss the reported MOC transports from the two latitudes. In section 4, we diagnose the hydrographic changes that give rise to the changes in the calculated transports. Finally, in section 5 we conclude and highlight the key issue of the choice of reference level for transport estimates.

2 Data & Methods

Data used here are from two mooring arrays in the Atlantic: the RAPID Climate Change (RAPID) and Meridional Overturning Circulation and Heat transport Array (MOCHA) moored observations at 26.5°N from 2004–2015 and the Meridional Overturning Variability Experiment (MOVE) moored observations at 16°N from 2000–2016 (Fig. 1). Both arrays were designed to estimate the strength of the overturning circulation using boundary measurements, but there are significant differences in their approaches to estimating the MOC (detailed below).

2.1 RAPID 26°N observations

At the western boundary at 26°N, the primary dynamic height observations are from a full-depth mooring in 4000 m at 26.5°N, 76.75°W (WB2). Below 4000 m, instrument records are taken from nearby (within 25 km) moorings, including WBH2 and WB3. Temperature and salinity records from individual instruments are vertically interpolated to form a western profile of hydrographic data as described in *McCarthy et al.* [2015]. During November 2005 to March 2006, the WB2 mooring failed, and so during this period, data from the WB3 mooring at 26.5°N, 76.5°W were substituted. Typical instrument configurations on this mooring include 18 MicroCAT (Sea-Bird Electronics, Bellevue, WA) records between 50 and 4800 dbar, though specific instrument locations and sampling intervals have varied over the 10 years of observations. Field calibrations are carried out

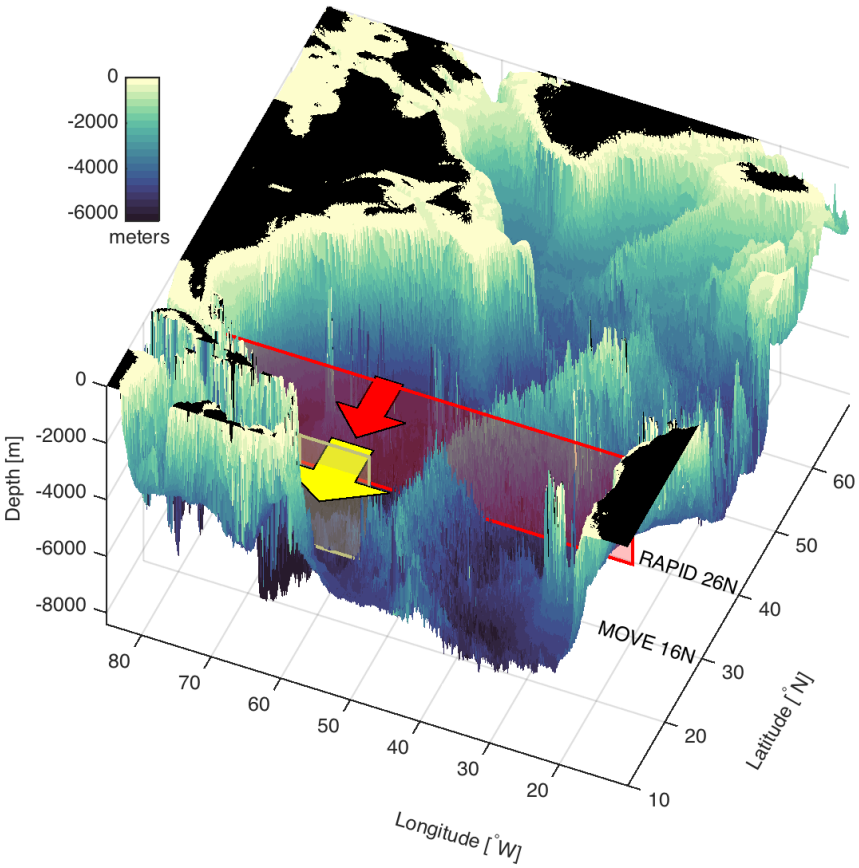

Figure 1. Moored observations at RAPID 26°N and MOVE 16°N. Bathymetry is shaded in color. The coloured boxes indicate the regions where transport is estimated by the two arrays.

on individual instruments by mounting them to the conductivity-temperature-depth (CTD) rosette for pre-deployment and post-deployment casts. MicroCAT measurements are compared to those from the CTD at bottle stops, with drifts between the pre-deployment and post-deployment casts used to offset the time series observations. Individual instrument records are filtered with a 2-day low pass filter to remove the tides before gridding vertically to 20 m resolution. Full details of the data processing can be found in *McCarthy et al.* [2015].

The MOC at 26°N is calculated by combining the *in situ* moored observations with estimates of the Florida Current transport and surface meridional Ekman transport. In this way, there is a depth-resolved estimate of transport spanning the Atlantic from Florida to the Canary Islands. The *in situ* moored observations are used to calculate dynamic height profiles relative to 4820 dbar, from which geostrophic shear is calculated by differencing dynamic height profiles (east minus west) across zonal sections of the array as

$$T_{int}(p) = \frac{\Phi_{east}(p) - \Phi_{west}(p)}{f} \tag{1}$$

where f is the Coriolis parameter, and Φ_{east} and Φ_{west} the dynamic height anomalies at a given pressure level p relative to zero at 4820 dbar at the east and west of the Atlantic,

respectively. Dynamic height is estimated from measured density profiles as

$$\Phi(p) = \int_{4820}^{p} \delta(p')\,\mathrm{d}p' \tag{2}$$

where δ the specific volume anomaly $(1/\rho)$. In a geostrophic calculation, a choice of reference level (level of no motion) or barotropic velocity (level of known motion) must be applied. At 26°N, the deepest common level between moorings (4820 dbar) is used as an initial reference level, assuming it is a level of no motion. These geostrophic transports are then combined with the net northward Florida Current (about 31 Sv), the net northward meridional Ekman transport (about 3 Sv) to produce a net transport estimate across the section every 12 hours. However, the net transport across the section calculated in this way is non-zero (and can be on the order of 10 Sv). Since it is aphysical that the Atlantic has a net northward transport of 10 Sv persisting over days to months, this indicates that 4820 dbar is not a level of no motion (zero flow). To compensate for the net transport across the section, zero mass transport across the section is assumed and a flow in the equal and opposite direction is applied. This flow is applied uniformly across the section (equal velocity at each depth and longitude), resulting in a width-weighted profile of transport-per-unit depth. Applying a compensation velocity in this way is consistent with the geostrophic shear calculation—a depth-independent velocity would not be measured by the ocean density variations. Equal distribution across the section is the simplest choice for how the velocities are distributed.

After this compensation transport profile is applied to the geostrophic transports between the Bahamas and Canary islands, the transport-per-unit depth is accumulated from the bottom to top. By construction, the integral is zero at the bottom and top. The depth where the transport is maximized is called the depth of maximum overturning, and the value at that depth is the value of the MOC. In this way, the MOC transport value is equal to the sum of the northward flowing waters above the depth of maximum overturning (about 1100m, but varies in time), and equal but opposite to the sum of the southward flowing waters below this depth.

2.2 MOVE 16°N observations

The main western mooring site of the MOVE 16°N array is MOVE3, a single, subsurface mooring that was initially deployed in early 2000 and has been in operation ever since. The location is approximately 16.3°N, 60.5°W, at 5000 m water depth a short distance east of Guadeloupe. Measurements of temperature, salinity, and currents are made from this platform [*Kanzow et al.*, 2006]. Instrumentation has varied over the years; the present configuration has 21 MicroCAT instruments for temperature and salinity covering the depth range from 50 m to the seafloor. Earlier deployments only covered the deeper layers below 1000 m.

Removal of sensor drift is done with CTD casts before deployment and after recovery [*Kanzow et al.*, 2006], identical to the 26°N array. The calibrated, quality-controlled data are made publicly available through the OceanSITES data portals (www.oceansites.org). Data available at OceanSITES also includes six additional sites where MOVE has made observations, two of which are still in operation and together with MOVE3 have formed the core array since early 2000 [*Send et al.*, 2011]: MOVE1 is near the Mid-Atlantic Ridge at 51.5°W and has MicroCAT instruments like MOVE3, and MOVE4 is a short distance west of MOVE3 and carries current meters to directly capture the boundary current.

The MOC at 16°N is calculated as the deep southward-flowing transport across the array between pressure levels of 1200 and 4950 dbar. The transport is computed as the sum of two components [*Kanzow et al.*, 2006]: a "boundary" component from direct current meter measurements at MOVE3 and west of it at MOVE4, an "internal" component using dynamic height profiles at MOVE3 and the eastern MOVE1 site referenced to zero flow at depth. While an "external" component can be derived from seafloor pressure ob-

servations at MOVE1 and MOVE3, they cannot be used to analyze low-frequency variability due to required de-trending [*Kanzow et al.*, 2006]. Since low-frequency variability is absent in the external component by construction, it is instead assumed that zero flow is a good approximation for slow changes at the 4950 dbar depth. This level coincides with the interface depth between northward-flowing Antarctic Bottom Water (AABW) and southward-flowing North Atlantic Deep Water (NADW). The array, being west of the Mid-Atlantic Ridge, explicitly assumes that the southward-flowing NADW is concentrated in the western half of the basin. The assumptions regarding the reference level and use of only the western basin were validated through numerical simulations early on in the project [*Kanzow*, 2004; *Kanzow et al.*, 2006]. In the original representation of southward MOVE transports as negative numbers, stronger flow corresponds to stronger negative numbers. For a more straightforward comparison with the transports at 26°N, here we flip the sign of the reported MOVE 16°N overturning to make stronger flow show as stronger positive.

2.3 Time series processing

Data from both 26°N and 16°N were bin-averaged into monthly time series. In order to focus on interannual and longer-term variations, a seasonal climatology was removed and time series were filtered with an 8-month Tukey window. While some sub-annual variations remain, the < 1-year filter window permits better identification of the timing of changes. In calculating correlations between time series, statistical significance was based on two-tailed t-tests where the numbers of degrees of freedom were determined from the integral time scale of decorrelation (Emery and Thomson, 2004).

2.4 Differences in MOC methodology at 16°N and 26°N

Two major differences exist between how the two arrays determine the strength of the MOC. First, at 16°N, the array extends eastward only to the Mid-Atlantic Ridge while at 26°N, it extends eastward to Africa. This was justified by observing system simulation experiments (OSSEs) at 16°N which showed that on longer timescales (4+ years), transport fluctuations at 16°N are primarily due to density changes at the western boundary [*Kanzow*, 2004]. This assumption is further supported by the 26°N observations that have shown that the western boundary dominates transport variability on interannual and longer timescales [*Frajka-Williams et al.*, 2016].

The second difference is the way in which variability at the reference level is addressed. Traditionally, geostrophic shear is referenced to a level of no motion, where the dynamic height is reference to a level where flow is weak or absent, and so the calculated geostrophic velocity is zero at this depth [*Talley et al.*, 2011]. At 16°N, this is applied as a constant-in-time deep level of no motion (4950 dbar), while at 26°N, the shear is referenced to a deep level of no motion (4820 dbar), but transports are later adjusted by a barotropic velocity profile (applied hypsometrically, or uniformly across the section). This compensation is chosen to ensure zero net mass transport across the latitude section, and is effectively the same as applying a time-varying deep velocity across 26°N.

In the following analysis (§3), we will evaluate the two MOC time series for the different latitudes as published, but removing the contribution of meridional Ekman transport from the MOC at 26°N. However, the differences in methods introduce uncertainty in making direct comparisons between the two. Following this initial analysis, we will focus on how the calculated transports change as a consequence of measured hydrographic changes.

3 MOC transports at 16°N and 26°N

At 26°N over the period Apr 2004 to Oct 2015, the MOC transport was 16.9 ± 3.4 Sv (as mean ± standard deviation, Fig. 2). Over the full MOVE record (Feb 2000 to Feb 2016), the mean overturning strength at 16°N is 24.1 ± 4.0 Sv, while over the 11.5-year overlap period (Apr 2004 to Oct 2015), the mean at 16°N is 24.1 ± 4.2 Sv. Here, the standard deviations were calculated on monthly binned time series. While these estimates suggest the overturning is 7 Sv stronger at 16°N than at 26°N, the array at 16°N is designed to capture the variability of the overturning rather than the mean. A small portion (about 1 Sv) of the difference in the mean between the two transports can be attributed to a throughflow at 26°N that is not accounted for in the zero net mass transport assumption; there is about 1 Sv of net throughflow from the Pacific, through the Arctic and southward in the Atlantic associated with the Bering Strait throughflow. Including this throughflow would slightly increase the southward deep flow at 26°N.

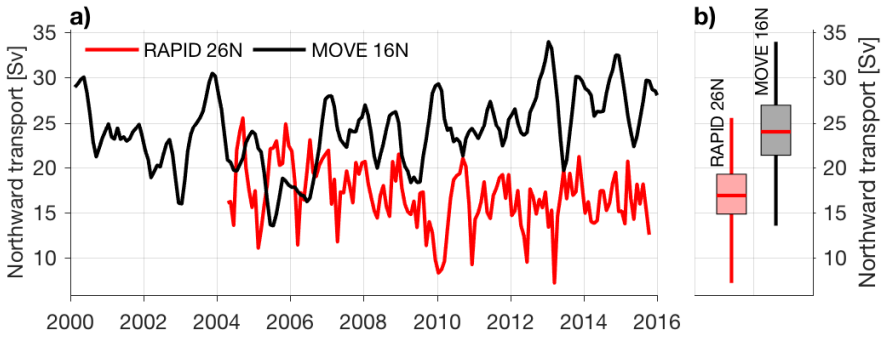

Figure 2. (a) Time series of meridional overturning circulation strength at 16°N (black) and 26°N (red) in the Atlantic. Transport is reported as positive for northward flowing water above the depth of maximum overturning. (b) The variability of the monthly time series as a box plot, where the horizontal line notes the median, the box the middle quartiles, and the vertical line the full range.

The long term tendencies at the two latitudes also differ. At 26°N the strength of the overturning has been reported as decreasing [*Smeed et al.*, 2014; *Frajka-Williams et al.*, 2016] at a rate of about 0.5 Sv/year, far exceeding that found in climate model variations [*Roberts et al.*, 2014]. Using the deseasonalized, 8-month filtered time series, we find that over the overlap period of April 2004 through Oct 2015, the 26°N MOC shows a decrease of 3.7 Sv (Fig. 3), with a slope of −0.37 ± 0.34 Sv/yr. The overturning at 16°N, on the other hand, shows an increase of 8.1 Sv—more than double the rate of decline at 26°N, where the trend is 0.81 ± 0.56 Sv/yr. Here, confidence intervals are reported for 90% confidence on the slope following, e.g. *Sveshnikov* [1968] and using the integral timescale of decorrelation [*Emery and Thomson*, 2004] to calculate the number of degrees of freedom (7.7 at 16°N and 8.7 at 26°N). A net convergence of only 1 Sv for a year would result in a sea level increase of about 5 m (based on 5 years and an area of 1000 km× 6000 km between the two latitudes). These transports suggest that deep southward flow at 16°N has increased relative to the deep southward flow at 26°N by more than 11 Sv. How can we reconcile these differences in transport?

Some of the difference may be that the net transport across all of 16°N is not measured (Fig. 1). Deep transports east of the mid-Atlantic ridge are also neglected. For these unmeasured transports to make up the difference between 16°N and 26°N, there would need to be northward flowing NADW in the eastern basin which recirculates southward in the west, contributing to the southward transports measured by the MOVE array west of the Mid-Atlantic Ridge. This flow would, however, need to cross the Mid-Atlantic Ridge in order to supply the deep transport west of the Mid-Atlantic Ridge; it may be possible

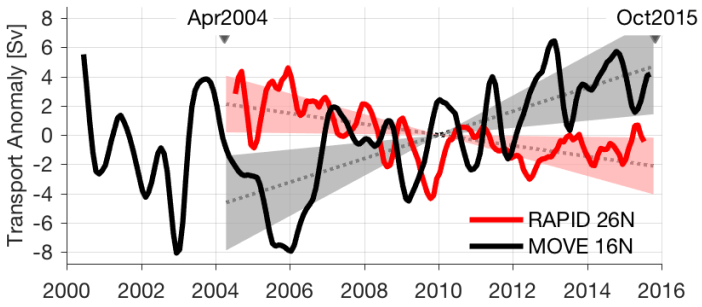

Figure 3. Transport time series (8-month low pass filter) and trends for the Atlantic MOC anomaly at 26°N and 16°N. Trends are computed over the overlap period (April 2004 through October 2015) and are shown with uncertainties on the trend calculated for 90% confidence. Confidence intervals were calculated as $\pm t_{0.1}^{n-2}\hat{\sigma}_b$ where $t_{0.1}^{n-2}$ = 1.91 for 26°N and 1.96 for 16°N. Number of degrees of freedom (n) were calculated using the integral timescale of decorrelation. Uncertainty on the slope estimate ($\hat{\sigma}_b$) was computed as $\hat{\sigma_e}/\sqrt{n}\sigma_t$ following e.g., *Sveshnikov* [1968].

for some deep flow to cross the Mid-Atlantic Ridge through deep channels (e.g., the Kane Fracture Zone at 24°N), though we do not explore this possibility further here. It is highly unlikely that the difference between the arrays would be made up by additional NADW formation between 16°N and 26°N, contributing to the enhanced southward flow at 16°N. However, one could envision that changes to the largely unmeasured AABW flow or deep volume storage/release could contribute to the difference.

Transports are, however, highly sensitive to the choice of a geostrophic reference level. Changing the deep reference velocities by just 1 mm s^{-1} across an ocean section 6000 km wide and 4000 m deep results in a transport change of 24 Sv (0.001 m/s×6000 km× 1000 m/km × 4000 m). The difference in transports between 16°N and 26°N may critically come down to the treatment of the reference level. While the deep level of no motion at 16°N was supported by the comparison of deep-referenced velocities with *in situ* bottom pressure measurements [Fig. S5 in *Send et al.*, 2011], this comparison was only possible on sub-annual timescales. On longer timescales, bottom pressure records are subject to instrumental drift [*Watts and Kontoyiannis*, 1990].

It is beyond the scope of the current paper to recommend adjustments to the method of estimating overturning from dynamic height mooring arrays and the application of a geostrophic reference level. These are important and broad questions which cannot be conclusively answered by the available observations. Instead, we will focus on what the observations can tell us, how they compare between the two latitudes, and how (after demonstrating striking similarities in the observed tendencies at the two latitudes) the opposing tendencies in transport arise. These investigations will make clear the importance of the treatment of deep reference level, but will also give insight into how the baroclinic circulation in the deep North Atlantic has been changing coherently on interannual to decade-long timescales.

3.1 Dynamic height changes

At both latitudes, the interior basin transports are calculated from dynamic height differences between the west and east but also current meter measurements very near (within 25 km of) the western boundary. The direct current meter measurements contribute little to the deep transport (not shown), so we will not consider them further. To identify the origin of the transport variations, we will separate equation (1) into the eastern and western side. Several previous investigations have considered the eastern and

western boundary sources separately, to better identify dynamic origins of transport changes [see for example *Kanzow et al.*, 2010; *Duchez et al.*, 2014; *Elipot et al.*, 2014]. For the purposes of a more direct comparison between 16°N and 26°N, we reference dynamic height to zero at 4820 dbar at both arrays and neglect fluctuations below 4820 dbar, including any northward flowing AABW. These transports are expected to be small (~1 Sv at 26°N) with small variations [standard deviation of 0.4 Sv over 6 months *Frajka-Williams et al.*, 2011; *McCarthy et al.*, 2015]. Note that while we are using western boundary dynamic height measurements, this is not the same as the deep western boundary current (DWBC) which is considered to be the intensified southward flow found near the western boundary. The data shown here represent transbasin transports (or partial transbasin transports, in the case of 16 N), which encompass both the DWBC and interior flow.

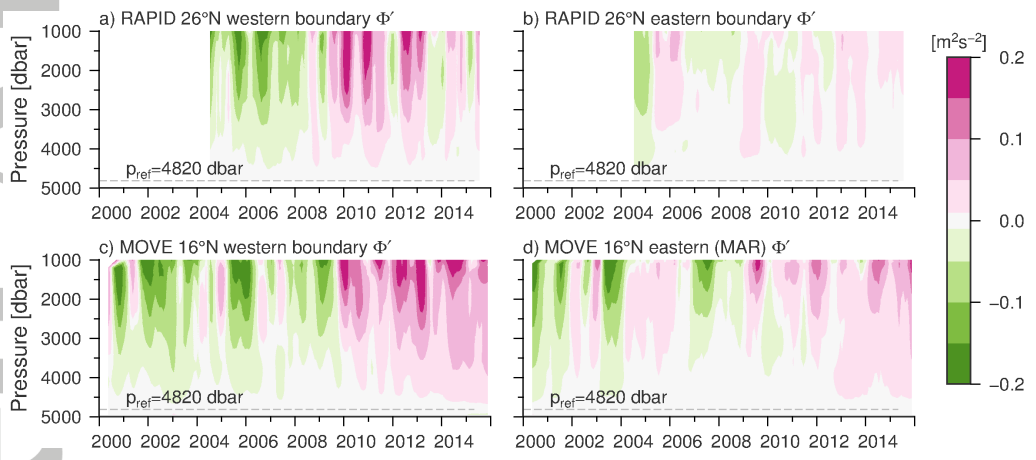

Figure 4. Dynamic height anomalies at the (a) western boundary and (b) eastern boundary of RAPID 26°N and (c) western boundary and (d) west of the MAR at MOVE 16°N. In all cases, dynamic height is referenced to zero at 4820 dbar (grey dashed line). A transition from negative (green) to positive (pink) dynamic height anomaly at 1000 dbar indicates a relatively strengthening of the southward upper NADW (1000–3000 dbar) relative to the southward lower NADW (3000–5000 dbar).

In the west at both latitudes, there is a clear shift from low to relatively higher dynamic height anomalies (Fig. 4a,c), where higher dynamic height corresponds to waters of lighter density. Notably, the shift is of the same sign at both latitudes. The transition from low-to-high occurs around 2009 at 26°N, and some months later at 16°N. Dynamic height anomalies are zero at 4820 dbar by construction, with an increasing amplitude relative to the bottom. The rate of change of dynamic height anomaly with depth appears to increase across the depth range 2000–3500 dbar, which would indicate that density anomalies in the range 2000–3500 dbar are responsible for changes in shear through equation (2).

In contrast, dynamic height anomalies at the eastern boundary of 26°N (off the Canary islands) show markedly weak interannual variability (Fig. 4c), indicating little to no density fluctuations or contribution to the transbasin shear. This suggests that Φ_{west} dominates equation (1) for 26°N [consistent with previously reported transport fluctuations in *Frajka-Williams et al.*, 2016]. The eastern limit of the 16°N array is at the western flank of the Mid Atlantic Ridge; here, fluctuations are only slightly weaker than at the western boundary of 16°N, and the dynamic height anomalies also show a tendency from negative to positive (Fig. 4d).

3.2 Dynamic height contributions to shear

To quantify the fluctuations in shear at both latitudes—independent of the choice of reference level—we calculate the dynamic or geopotential thickness between two depths (Fig. 5). At the western boundary of both 16°N and 26°N, the thickness anomaly has shifted from negative to positive (Fig. 5a). The dynamic thickness anomaly is also calculated at the east (Fig. 5b). At 26°N, the deep dynamic height variability is negligible in the east. At 16°N, there are a few larger variations in 2007 and 2009, but since 2004, the eastern boundary dynamic thickness anomaly has been relatively smaller than at the west. Comparing the two 5-year periods (2004–2009 and 2009–2014), the dynamic thickness in the west of this layer at 16°N changed from 11.65 ± 0.07 to 11.79 ± 0.08 m^2s^{-2} (mean ± standard deviation calculated on monthly binned time series). At 26°N, the change was from 11.82 ± 0.05 to 11.96 ± 0.07 m^2s^{-2}. At both latitudes, the geopotential thickness change or shear increased by about 0.14 m^2s^{-2}. In the calculation of transport, equation (1) applied to both latitudes, the transport tendency will be towards more negative transports at 1200 dbar relative to 4000 dbar.

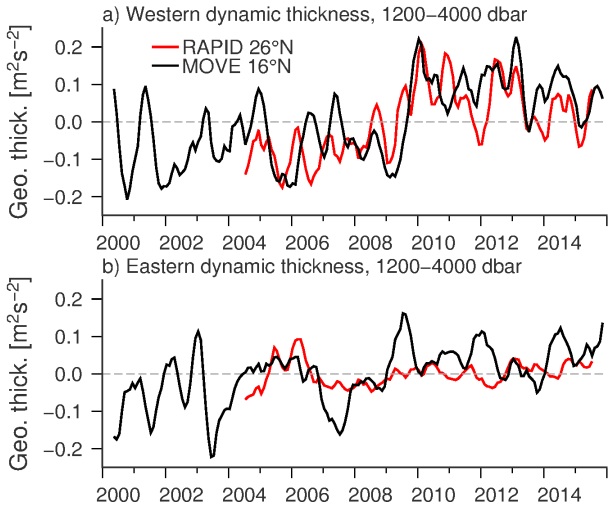

Figure 5. Dynamic thickness anomaly time series at (a) the western boundary of RAPID 26°N and MOVE 16°N and (b) the eastern boundary of RAPID and the eastern mooring of MOVE (west of the Mid-Atlantic Ridge).

Using equation (1) replacing Φ_{east} with its time-mean, we can estimate the velocity profile due to dynamic height variations at the west only (Fig. 6). At both latitudes, the dynamic height changes from prior to 2009 to more recent periods give a consistent strengthening tendency of the southward flow in the upper NADW (1100–3000 dbar) layer. We can further see that this transition occurred relatively abruptly in 2009, with the velocity profiles grouping into two clusters for before and after.

Shear in the transport due to dynamic height anomalies at the west (Φ'_{west}) can also be estimated between the two layers (1100–3000 m and 3000–5000 m) by scaling by f and integrating in depth as

$$\mathbf{V}_z = \int_{3000}^{1100} \frac{-\Phi'_{west}}{f}\,\mathrm{d}z - \int_{5000}^{3000} \frac{-\Phi'_{west}}{f}\,\mathrm{d}z \qquad (3)$$

where the first integral represents the transport contribution from the intermediate layer (upper NADW), and the second integral from the lower layer (lower NADW). For the period Feb 2000–April 2001, MOVE data in the west are absent between 1100 and 1200

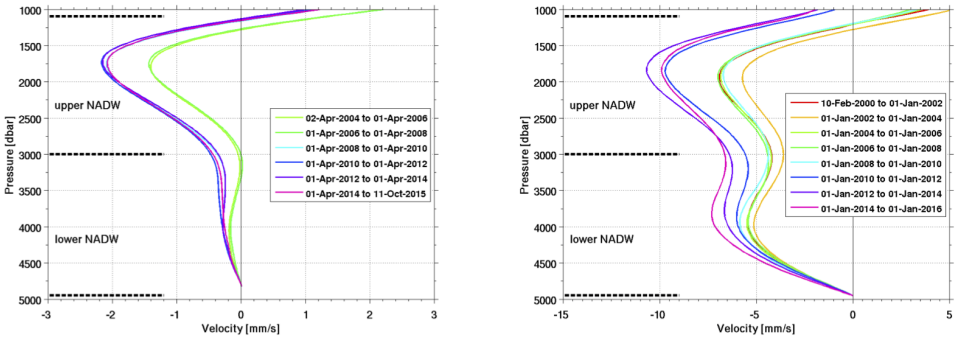

Figure 6. Velocity estimates derived from dynamic height anomalies calculated at the western boundary profiles from (a) RAPID 26°N and (b) MOVE 16°N, following *Send et al.* [2011]. Dynamic height anomalies were integrated relative to a deep reference level.

dbar, so these have been filled in with the time-mean profile. Computing $\mathbf{V}_z$ at both latitudes gives a sense of the change of the circulation in units of Sv, where a positive value represents a strengthening of the upper NADW transports relative to the lower NADW transports (Fig. 7). Between the two five year periods, both latitudes showed an increase in the shear transport of 3.9 Sv (MOVE 16°N) and 2.6 Sv (RAPID 26°N). Note that while the geopotential thickness anomaly at the two latitudes was similar, f is smaller at 16°N resulting in a larger transport anomaly.

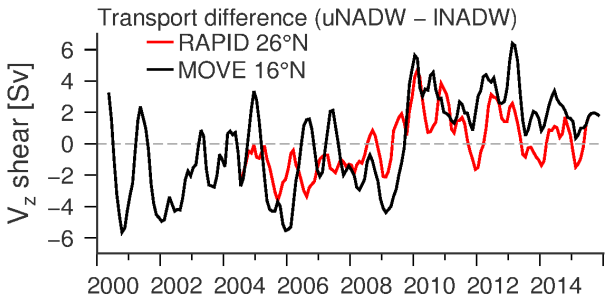

Figure 7. Shear anomaly due to western boundary dynamic height changes as in equation (3) for MOVE at 16°N (black) and RAPID at 26°N (red). The observed dynamic height anomalies represent an increase in $\mathbf{V}_z$ by about 3.9 Sv (MOVE) and 2.6 Sv (RAPID) between the two 5-year periods, 2004–2009 and 2009–2014.

These results show that the observed dynamic height changes at the western boundary of the Atlantic are consistent in tendency (towards positive thickness anomaly) and timing (between 2009–2010) at both latitudes. This results in the same sign effect on changes to the geostrophic transport, T_{int}, relative to a deep level of no motion. The effect of these changes is to intensify the shear between the lower and upper NADW layers (Fig. 6 & 7). At 16°N, this directly translates into a strengthening of the estimated MOC. The velocity profiles from Fig. 6 are integrated below 1200 m, and the latter half of the period shows stronger southward flow. As a consequence, the estimated MOC has strengthened. At 26°N, the shear profiles are combined with a time-varying hypsometric compensation before transports are estimated. First, we investigate the origin of the shear changes in the western boundary (§4).

4 Hydrographic changes at the west in the Atlantic

Temperature-salinity (T-S) diagrams of water mass properties at 26°N and 16°N show variations from warm and salty in the thermocline to cold and fresh at depth, with only a modest change in slope of the T-S relationship around 2000 m (Fig. 8). This bend in the curve corresponds to the transition between central Labrador Sea Water (cLSW) and Iceland-Scotland overflow water [ISOW *van Sebille et al.*, 2011]. At 26°N, in the recent 10 years, the waters below 1100 m have tended towards cold and/or fresh on all isopycnals with the exception of at 2000 m (cLSW) where the properties have remained the same. At 16°N, properties at all depths have tended towards cold and fresh on isopycnals below 1100 m. These changes are consistent with, but have smaller amplitude than, the cooling and freshening observed at 26°N from hydrographic sections over the period 1984–2010 [*van Sebille et al.*, 2011].

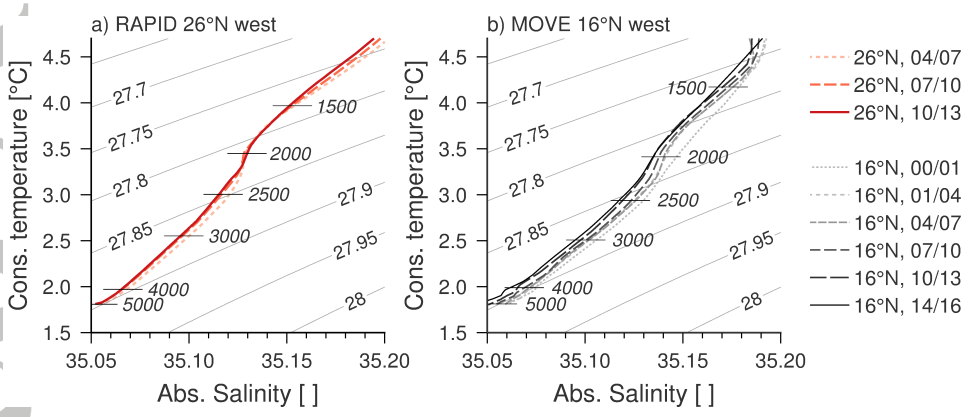

Figure 8. 3-year averages of the monthly binned conservative temperature and absolute salinity, where 00/03 indicates the period October 2000 through September 2003. Contours are the σ_0 densities. Average depths are indicated by the black lines.

In the vertical, temperature profiles decrease to a minimum of about 1.8°C at 26°N and 1.9°C at 16°N (Fig. 9). Salinities at both latitudes are fresher at depth than in the thermocline. At mid-depths, warmer, saltier waters are found (around 3°C and 35.1 around 2000 m). Over the 11-year RAPID deployment and 16-year MOVE deployment, the waters at depth (below 1000 m) have tended towards fresher water; temperature changes on depth surfaces are more ambiguous, with temperatures below 3500 m cooling at 16°N but warming at 26°N.

Comparing the average properties between 1200 and 4650 dbar between two complete five-year periods of observations, Apr 2004–Mar 2009 and Apr 2009–Mar 2014, temperatures warmed at 26°N by 0.023°C, from 2.77 ± 0.03 to 2.79 ± 0.03°C, while salinities freshened by 0.002, from 35.104 ± 0.002 to 35.103 ± 0.002 (mean ± standard deviation on the monthly binned time series). At 16°N, over the same two five-year periods, temperatures between 1200–4650 dbar warmed by 0.018°C, from 2.81 ± 0.03 to 2.83 ± 0.03°C. Salinities freshened by about 0.003, from 35.111 ± 0.002 to 35.108 ± 0.003. At both latitudes, the warming and freshening results in lighter (less dense) waters at the western boundary at depth. While observed changes are near the estimated accuracy of measurements [*McCarthy et al.*, 2015], the shift in properties between the two periods is statistically significant, and contributes to changes in density and dynamic height.

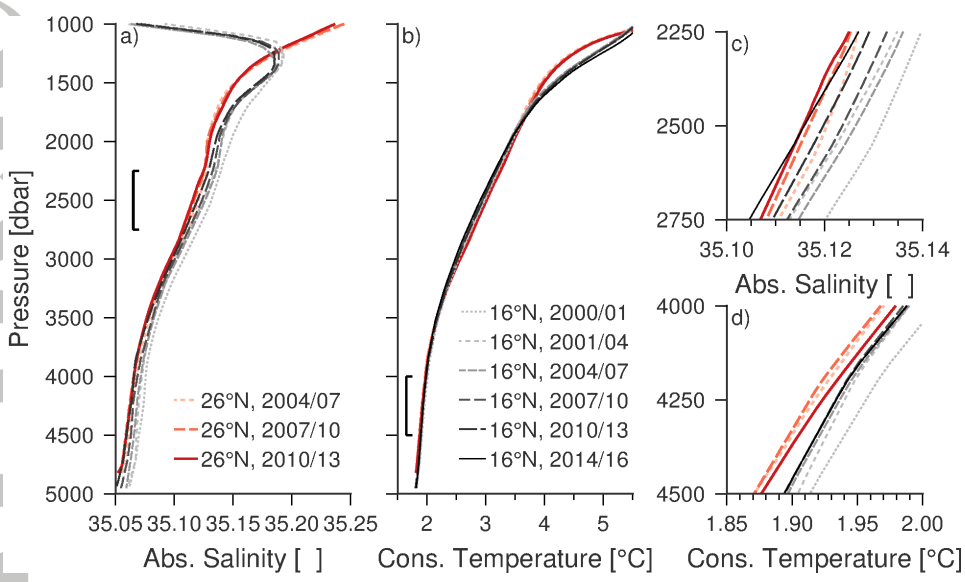

Figure 9. (a) Absolute salinity and (b) conservative temperature profiles from the western boundary of the RAPID 26°N and MOVE 16°N, in red and grey tones, respectively. Darker colours indicate later 3-year averages as in Fig. 8. Panels (c) and (d) are insets of salinity and temperature for the depth ranges 2250–2750 and 4000–4500 dbar, respectively.

Density variations

The effect of T-S variations on transport is through density. Above, we saw that there was a consistent tendency towards freshening at both latitudes, but did not investigate the timing of those changes. We will do this with density, but first will investigate the vertical coherence of density anomalies at each latitude to gain insight into the depth-structure of density fluctuations. At each depth, we compute a time series of the density anomaly from the time mean. These anomaly time series are then correlated with each other to identify covariability between density anomalies at different depths. Fig. 10 shows the correlation coefficient between density anomalies at one depth (x-axis) with those at another depth (y-axis). Since density anomalies at the same depth are exactly correlated (correlation coefficient of 1), the 1-1 axis from upper left to lower right is exactly 1. Broader patches of high correlation around this axis are found for 26°N in the depth range 1100–4800 m and for 16°N in the range 1200–4650 dbar. This means, for example, that density anomalies at 2000 m co-vary with density anomalies at 4000 m. Overall, it suggests that density anomalies everywhere below 1200 m co-vary, or similarly, that the time series of density anomalies at a single depth will represent the variability for the whole deep layer. In contrast, in the thermocline above 1200 m, the red areas of co-variability contract back together towards the 1-1 diagonal (Fig. 10), indicating that density anomalies above 1200 m do not co-vary with density anomalies below 1200 m.

The high degree of covariability below 1200 m simplifies the comparison of density anomalies between latitudes, because it means that density fluctuations are largely coherent below 1200 m and the comparison between latitudes will not strongly depend on a particular choice of depth. It also gives confidence in calibrations and sensor stability. Based on these results, we may be able to apply a layered approximation of the ocean, with a small number of layers (2–3) explaining a large fraction of the observed density and transport variations.

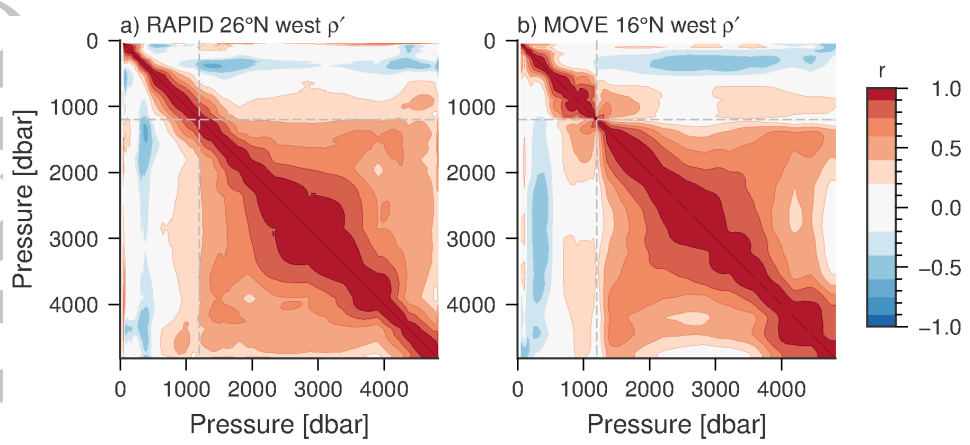

Figure 10. Correlation between density anomalies at each depth from (a) the western boundary of RAPID 26°N, and (b) the western boundary of MOVE 16°N. Red colours indicate positive correlation (coherent variations) while blue colours indicate negative correlation (anti-phase variations). Grey dashed lines are at 1200 m.

While the time series of observations are relatively short for investigating interannual variations, we investigate the relative timing of changes at the two latitudes by calculating a lag-correlation between density anomaly time series at each depth (Fig. 11a). Above 1200 m, there is little to no relationship between density anomalies at 26°N and 16°N. Between 1200 m and 4650 m, density anomalies are correlated, with anomalies at 16°N tending to occur simultaneously or after those at 26°N. Highest correlations are for RAPID 26°N leading MOVE 16°N by less than 1 year, with a secondary region of elevated correlation around 24 months (RAPID leading MOVE) for densities below 3500 m. The strongest correlations occur around 1500 bar and 3500–4000 bar. Fig. 11b shows an example of a time series of density anomalies at 3800 dbar from RAPID 26°N and MOVE 16°N, with the time series from 26°N shifted later by 7 months, which gives the maximum correlation. Both latitudes show a transition from relatively dense to relatively light waters at the end of 2009 at 16°N (and 7 months earlier at 26°N). These shifts are of the same sign and similar magnitude at the two latitudes and are directly responsible for the increase in dynamic height anomaly over the same period. Seven months corresponds to a speed of order 10 cm/s. This is about ten times faster than the overall speed of advection between the Labrador Sea and 26°N [*van Sebille et al.*, 2011], but this is not surprising when compared to model results showing a faster adjustment over the subtropics than from the subpolar to subtropical gyre [*Zhang*, 2010].

5 Constructing the MOC at 26°N - reversing the trends

From the moored profiles of temperature and salinity, we have seen that a deep freshening occurred at both 16°N and 26°N, leading to a decrease in deep densities, and through it, an increase in dynamic height anomalies at the western boundary. This has contributed to a strengthening of the deep shear at both latitudes, occurring around the end of 2009 at 16°N, and a few months earlier at 26°N. At MOVE 16°N, the resulting strengthening of the upper NADW layer (Fig. 6) directly translates into a strengthening of the southward MOC, as the MOC is calculated as the integral of the geostrophic shear profile between 1200 and 4950 m [*Kanzow et al.*, 2006; *Send et al.*, 2011].

At 26°N, however, the total transports across the section include both the geostrophic interior flow (T_{int}) but also the compensation term, so that the overturning (Ψ) includes

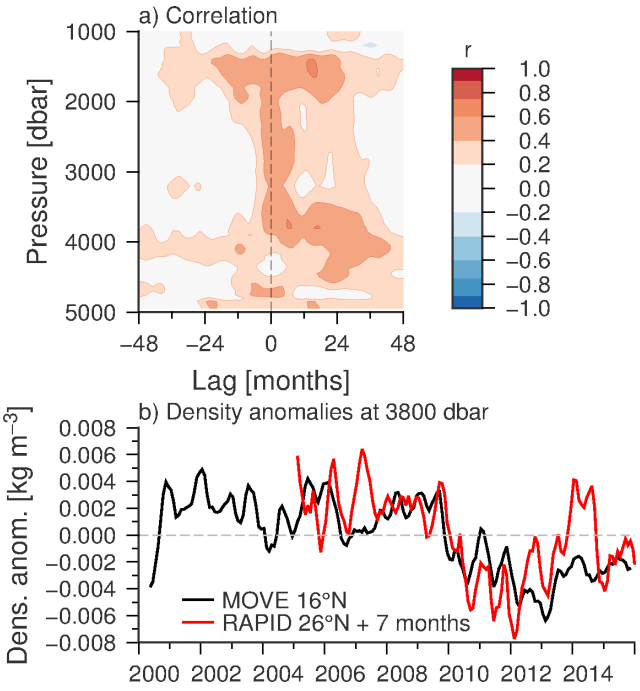

Figure 11. Lag correlation between density anomalies at different latitudes but the same depth. (a) Correlation coefficient between density anomalies at the western boundaries of MOVE 16°N and RAPID 26°N, as a function of depth (y-axis) and lag in months (x-axis). (b) Time series of density anomalies at the two latitudes, at 3800 dbar. The density time series from RAPID 26°N has been shifted forward in time by 7 months. Positive lag corresponds to 26°N leading 16°N.

contributions from multiple components as

$$\Psi = \int^{z} T_{gs} + T_{ek} + T_{wbw} + T_{int} + T_{comp}\, \mathrm{d}z \tag{4}$$

where T_{gs} and T_{ek} are the transports of the Florida Current and surface Ekman transport, respectively, and T_{wbw} is from direct current meter observations in the western wedge [*McCarthy et al.*, 2015]. T_{gs} and T_{ek} have little interannual variability over the 2004–2015 period (Fig. 12a). The changes we described above in dynamic height at the west result in an intensification of the southward geostrophic flow referenced to the bottom, shown in Fig. 12c. These are similar to the changes estimated at 16°N.

However, the geostrophic thermocline transports (Fig. 12b) also show an increase in the southward flow. The RAPID method applies a constraint of zero net mass transport across the section at 26°N, which appears in the T_{comp} term (Fig. 12a). Because the geostrophic transports are so large, particularly by the time the dynamic height anomalies have been integrated up to the top 1000 m, the compensation transport is large and in the opposite direction (showing a tendency towards less southward/more northward flow). This compensation transport is applied hypsometrically (i.e., uniform velocities at each depth and longitude), which means that when integrated over the NADW layer (1100–5000 dbar), roughly 80% of the compensation transport is applied to the deep flow. As a consequence, T_{comp} dominates over the geostrophic contribution T_{int} in the deep layer, resulting in the overall weakening of the overturning circulation seen in Fig. 2. Hence we see that while both arrays show the same tendency in the baroclinic (shear) fluctuations, towards enhanced southward flow in the UNADW layer relative to the LNADW layer, the application of the zero net mass transport constraint at 26°N reverses the tendency

of the MOC transport. Without the zero net mass transport constraint, using a deep and fixed level of no motion for the geostrophic transports, the MOC transport at 26°N shows a strengthening tendency.

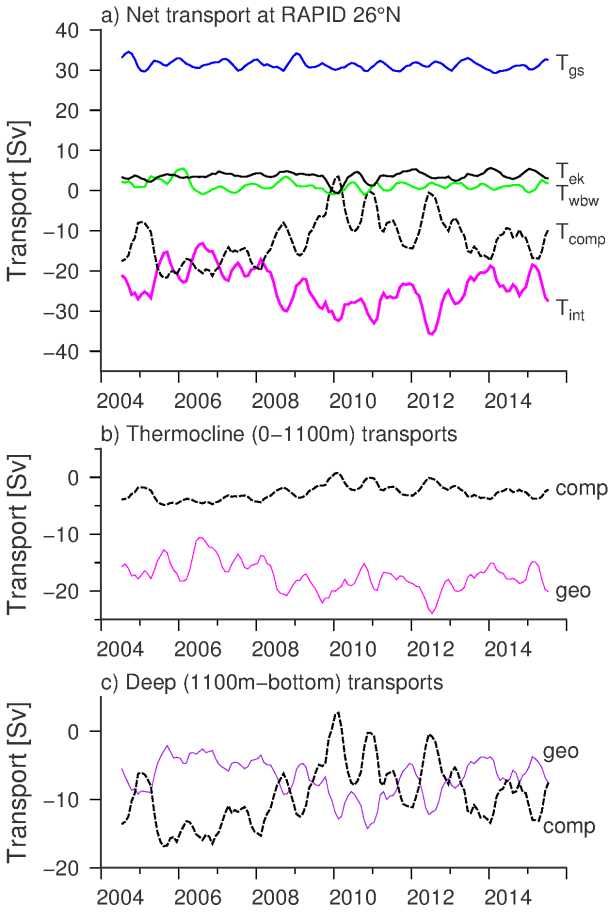

Figure 12. Total transports at 26°N, applying mass compensation. (a) Florida Current T_{gs} (blue), Ekman T_{ek} (black), western boundary current meter estimates T_{wbw} (green), geostrophic estimates T_{int}, relative to 0 at 4820 dbar (magenta) and external or compensation transport T_{comp} (black dashed). The sum of these is zero at all times. (b) Geostrophic transport in the thermocline (0–1100 m, magenta) relative to 0 at 4820 dbar, and the compensation applied over the 0–1100 m layer (black dashed). (c) Geostrophic transport in the deep layer (1100m–bottom) and the compensation applied over this layer (black dashed).

6 Conclusions, Discussion, and Outlook

Despite differences in methodology between the MOVE 16°N and RAPID 26°N boundary arrays for estimating ocean transport, there are coherent observable changes over the 11- and 16-year moored observations: When examined more closely, we see that both latitudes derive most of observed low frequency variability in calculated MOC transports from the western boundary densities. Both latitudes indicate a freshening of the deep layers at the west over the 2004–2014 period. This, in turn, contributes to a lighter deep density and thicker dynamic height anomaly at the west, with similar magnitudes and a shift at both latitudes around 2009–2010. These changes are computed directly from density observations, but may arise from either property changes (Fig. 8) or thickness/volume changes of a particular layer. The vertical coherence in the observed property changes,

and inter-array coherence give confidence that the measurement accuracy is sufficient to resolve the changes. This is a relevant point because the observed freshening signals are small and require careful calibration of the salinity sensors. The freshening signal results in a consistent change in the transbasin shear at each latitude. The vertical shear changed such that southward flow in the subtropical North Atlantic below 3 km weakened relative to the southward flow above, and this shift occurred between 2009–2010. These results show that the deep baroclinic circulation in the Atlantic—potentially the component of the circulation most relevant to changes on long time scales—is coherent between the two latitudes. There is a slight time offset between the two latitudes, such that fluctuations at 26°N lead those at 16°N, but this is based mostly on the 2009–2010 shift, i. e. one event.

While the transport observations at 26°N and 16°N both rely on the thermal wind equations (measuring density in order to calculate geostrophic shear), choosing an appropriate reference level to translate shear into absolute velocity remains a challenge. At 26°N, the reference level is applied as a barotropic compensation by assuming no net transport across the section on timescales longer than 10-days. At 16°N, the choice of no motion near 5000 m was validated by OSSEs and is consistent with bottom pressure measurements on shorter (sub-interannual) time scales. However, the transport tendencies in the published transports at MOVE 16°N and RAPID 26°N are in opposite directions [*Baringer et al.*, 2017], though the shear is trending in the same directions: here, we have shown that it is the application of reference levels that causes the difference. The 16°N transports suggest a strengthening of the overturning by about 8 Sv over the 2004–14 decade, while the 26°N transports indicate a weakening by about 4 Sv over the same period. Note that the methods employed at these latitudes to determine the overturning differ yet again from those used in other boundary arrays [e. g. *Toole et al.*, 2011, where the transport changes are identified in density space].

The application of reference levels is therefore a key element of estimating the overturning circulation through thermal wind balance. At 26°N, application of a zero net mass transport constraint resulted in a reversal in the estimated deep transport tendencies (from a strengthening southward deep flow, consistent with a strengthening MOC, to a weakening southward deep flow and reducing MOC). Estimates of the barotropic transport variability from PIES (Pressure inverted echo sounders) at 16°N support the use of a deep reference level, showing that even when incorporating deep pressure gradient fluctuations, the tendency of transport variability on timescales up to 2-years is not affected (Fig. 13, also Fig. S5 in *Send et al.* [2011]). Due to limitations of measuring long records of pressure in the ocean, the barotropic flow cannot be evaluated over longer timescales. On timescales where bottom pressure sensors can be used to estimate barotropic transports, the discrepancies in transports between MOVE and RAPID persist—i.e., the ocean is moving as shown by the individual arrays. However on longer timescales, there is a critical area of uncertainty in how best to incorporate a choice of reference level in the geostrophic shear method. This will likely introduce uncertainty in applying the shear method at all locations where a zero net mass transport assumption cannot be made. While the observational arrays at 16°N and 26°N were validated using OSSEs prior to deployment and verified with available datasets (including bottom pressure)—both elements of best practice in designing observational arrays for ocean transports—the results here demonstrate that methodological uncertainties remain in how to measure the large-scale ocean circulation.

Observations of the large-scale circulation at individual latitudes have revolutionized to our understanding of variations in the overturning circulation [*Srokosz and Bryden*, 2015]. However, efforts to relate the variability observed at different latitudes via different measurement designs have proved challenging [*Elipot et al.*, 2013; *Mielke et al.*, 2013; *Elipot et al.*, 2014]. A clear result of this analysis is that the baroclinic changes driven by the western boundary densities are consistent between the two latitudes. To reconcile the discrepancies between the derived transports, the remaining possible explanations are:

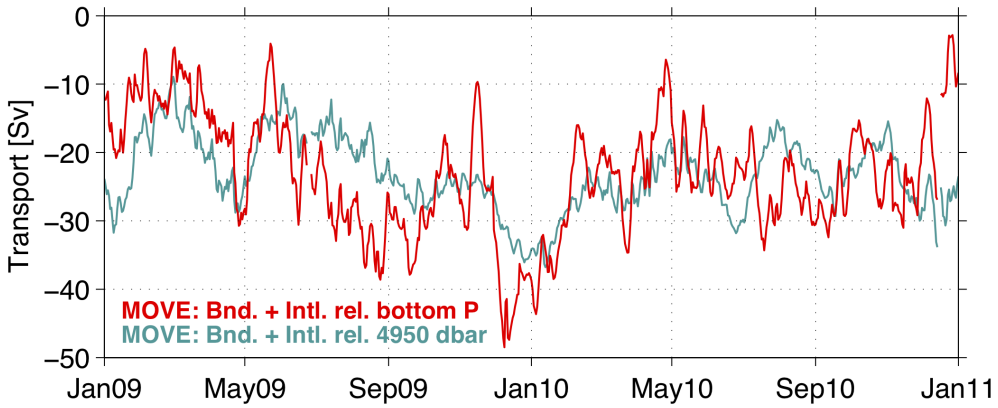

Figure 13. Transport estimates at 16°N with geostrophic transports referenced to 4950 dbar (green) and referenced to seafloor pressure as observed from PIES (red). The PIES data were processed with a low-pass filter (10-day running-mean) to remove tides, and then linearly detrended. The PIES deployments started in mid-2007 and mid-2008 for the eastern and western site, respectively, and lasted about four years each. The initial, more exponential, drift occurred before the time period shown in the figure. The southward anomaly in January 2010 occurs in both curves, and so is not an artefact of using a reference level of 4950 dbar in the green curve.

- that the oceanic variability, as manifested in the barotropic transport, is actually distinct at the two latitudes. This would be a dramatic departure from the picture of a coherent AMOC working like a connected cell across large parts of the ocean basin.
- that error estimates, observational assumptions, or measures of performance at either array are wrong or at least have overlooked important parts of the circulation. Given that both arrays have spent substantial effort validating their observational approaches and the underlying assumptions, it is becoming increasingly difficult to imagine, let alone find, where and what may have been missed.

Here, rather than attempting to modify the method for determining the reference level at individual latitudes, we investigate in detail the origins of the observed transport variability in order to better understand what the two arrays are measuring. In doing so, we have highlighted a known area of methodological uncertainty in estimating ocean transports: that of applying a choice of geostrophic reference level. New investigations are underway to determine uncertainties in the RAPID 26°N method of calculating overturning transports [*Sinha et al.*, 2018]. Recent advances using satellite-based estimates of ocean bottom pressure [*Bentel et al.*, 2015; *Landerer et al.*, 2015] show promise at providing independent estimates of deep ocean transport variability, but due to unconstrained trends in the satellite data, are not yet able to independently verify the deep ocean transports. These trends may be resolved as the satellite record increases in length, or could potentially be resolved by a combination of satellite and Argo-based datasets [*Willis and Fu*, 2008]. Sustained flow divergences or convergences between the arrays would also lead to basin-wide mass imbalances that might eventually be detectable. Whatever the solution to these discrepancies, they need to be addressed as a priority because these differences highlight either an inadequacy of the measurement methods or lack of understanding of the actual circulation patterns. The US AMOC program has called out identifying and explaining "coherent and incoherent signals between different study sites" as a priority [*Danabasoglu et al.*, 2016], and this study takes a step in that direction.

Acknowledgments

EFW was funded by a Leverhulme Trust Research Fellowship. JK was supported by NASA Headquarters under the NASA Earth and Space Science Fellowship Program - Grant NNX16AO39H Data from the RAPID Climate Change (RAPID)/Meridional Overturning Circulation and Heat flux Array (MOCHA) projects are funded by the Natural Environment Research Council (NERC) and National Science Foundation (NSF, OCE1332978), respectively. Data are freely available from www.rapid.ac.uk. The Meridional Overturning Variability Experiment (MOVE) was funded by National Oceanic and Atmospheric Administration (NOAA), the Climate Program Office–Climate Observation Division, and initially by the German Bundesministerium fuer Bildung und Forschung. MOVE and RAPID are part of the international OceanSITES program (www.oceansites.org). Florida Current transports are funded by the NOAA and are available from www.aoml.noaa.gov/phod/floridacurrent. Special thanks to the captains, crews, and technicians, who have been invaluable in the measurement of the MOC from moorings in the Atlantic over the past 18 years.

References

Baringer, M. O., D. A. Smeed, J. Willis, M. Lankhorst, W. R. Hobbs, S. Dong, G. McCarthy, D. Rayner, W. E. Johns, G. Goni, and U. Send (2017), Meridional overturning and oceanic heat transport circulation observations in the North Atlantic Ocean, in *State of the Climate in 2016*, vol. 98, edited by J. Blunden and D. S. Arndt, pp. S84–S87, B. Am. Meteorol. Soc.

Bentel, K., F. W. Landerer, and C. Boening (2015), Monitoring atlantic overturning circulation variability with grace-type ocean bottom pressure observations-a sensitivity study, *Ocean Sci. Disc.*, *12*(4), 1765–1791, doi:10.5194/osd-12-1765-2015.

Bingham, R. J., C. W. Hughes, V. Roussenov, and R. G. Williams (2007), Meridional coherence of the North Atlantic meridional overturning circulation, *Geophys. Res. Lett.*, *34*, L23,606, doi:10.1029/2007GL031731.

Black, R. (2010), Gulf Stream 'is not slowing down', *BBC News*.

Broecker, W. S. (1991), The great ocean conveyor, *Oceanography*, *4*, 79–89, doi:10.5670/oceanog.1991.07.

Cunningham, S. A., C. Roberts, E. Frajka-Williams, W. E. Johns, W. Hobbs, M. D. Palmer, D. Rayner, D. A. Smeed, and G. D. McCarthy (2013), Atlantic MOC slowdown cooled the subtropical ocean, *Geophys. Res. Lett.*, *40*, 6202–6207, doi:10.1002/2013GL058464.

Danabasoglu, G., S. Yaeger, and et al. (2014), North Atlantic simulations in Coordinated Ocean-ice Reference Experiments, phase II (CORE-II): Part I: Mean states, *Ocean Model.*, *73*, 76–107, doi:10.1016/j.ocemod.2013.10.005.

Danabasoglu, G., S. G. Yeager, W. M. Kim, E. Behrens, M. Bentsen, D. Bi, A. Biastoch, R. Bleck, C. Boening, A. Bozec, V. M. Canuto, C. Cassou, E. Chassignet, A. C. Coward, S. Danilov, N. Diansky, H. Drange, R. Farneti, E. Fernandez, P. G. Fogli, G. Forget, Y. Fujii, S. M. Griffies, A. Gusev, P. Heimbach, A. Howard, M. Ilicak, T. Jung, A. R. Karspeck, M. Kelley, W. G. Large, A. Leboissetier, J. Lu, G. Madec, S. J. Marsland, S. Masina, A. Navarra, A. J. G. Nurser, A. Pirani, A. Romanou, D. Salas y Melia, B. L. Samuels, M. Scheinert, D. Sidorenko, S. Sun, A.-M. Treguier, H. Tsujino, P. Uotila, S. Valcke, A. Voldoire, Q. Wang, and I. Yashayaev (2016), North Atlantic simulations in coordinated ocean-ice reference experiments phase II (CORE-II). Part II: Inter-annual to decadal variability, *Ocean Model.*, *96*, 65–90, doi:10.1016/j.ocemod.2015.11.007.

Dong, S., G. Goni, and F. Bringas (2015), Temporal variability of the South Atlantic meridional overturning circulation between 20°S and 35°S, *Geophys. Res. Lett.*, *42*, 7655–7662, doi:10.1002/2015GL065603.

Duchez, A., E. Frajka-Williams, N. Castro, J. J.-M. Hirschi, and A. Coward (2014), Seasonal to interannual variability in density around the Canary Islands and their

influence on the AMOC at 26°N, *J. Geophys. Res.-Oceans*, *119*, 1843–1860, doi: 10.1002/2013JC009416.

Elipot, S., C. Hughes, S. Olhede, and J. Toole (2013), Coherence of western boundary pressure at the RAPID WAVE array: Boundary wave adjustments or deep western boundary current advection?, *J. Phys. Oceanogr.*, *43*, 744–765, doi:10.1175/JPO-D-12-067.1.

Elipot, S., E. Frajka-Williams, C. Hughes, and J. Willis (2014), The observed North Atlantic moc, its meridional coherence and ocean bottom pressure, *J. Phys. Oceanogr.*, *44*, 517–537, doi:10.1175/JPO-D-13-026.1.

Elipot, S., E. Frajka-Williams, C. Hughes, S. Olhede, and M. Lankhorst (2017), Observed basin-scale response of the North Atlantic meridional overturning circulation to wind stress forcing, *J. Climate*, *30*, 2029–2054, doi:10.1175/JCLI-D-16-0664.1.

Emery, W. J., and R. E. Thomson (2004), *Data Analysis Methods in Physical Oceanography*, 2nd ed., Elsevier.

Frajka-Williams, E., C. C. Eriksen, P. B. Rhines, and R. R. Harcourt (2011), Determining vertical velocities from Seaglider, *J. Atmos. Ocean. Tech.*, *28*, 1641–1656, doi: 10.1175/2011JTECHO830.1.

Frajka-Williams, E., C. S. Meinen, W. E. Johns, D. A. Smeed, A. D. Duchez, A. J. Lawrence, D. A. Cuthbertson, H. L. Bryden, G. D. McCarthy, M. O. Baringer, D. Rayner, and B. I. Moat (2016), Compensation between meridional flow components of the Atlantic MOC at 26°N, *Ocean Sci.*, *12*, 481–493, doi:10.5194/os-12-481-2016.

Kanzow, T. (2004), Monitoring the integrated deep meridional flow in the tropical North Atlantic, Ph.D. thesis, Christian-Albrechts-Universit at, Kiel, Germany.

Kanzow, T., U. Send, W. Zenk, M. Rhein, and A. Chave (2006), Monitoring the deep integrated meridional flow in the tropical North Atlantic: Long-term performance of a geostrophic array, *Deep-Sea Res. Pt. I*, *53*, 528–546, doi:10.1175/JPO-D-12-067.1.

Kanzow, T., S. A. Cunningham, W. E. Johns, J. J.-M. Hirschi, J. Marotzke, M. O. Baringer, C. S. Meinen, M. P. Chidichimo, C. Atkinson, L. M. Beal, H. L. Bryden, and J. Collins (2010), Seasonal variability of the Atlantic meridional overturning circulation at 26.5°N, *J. Climate*, *23*, 5678–5698, doi:10.1175/2010JCLI3389.1.

Kelly, K. A., L. Thompson, and J. Lyman (2014), The coherence and impact of meridional heat transport anomalies in the Atlantic Ocean inferred from observations, *J. Climate*, *27*, 1469–1487, doi:10.1175/JCLI-D-12-00131.1.

Landerer, F. W., D. N. Wiese, K. Bentel, C. Boening, and M. M. Watkins (2015), North Atlantic meridional overturning circulation variations from GRACE ocean bottom pressure anomalies, *Geophys. Res. Lett.*, *42*, 8114–8121, doi:10.1002/2015GL065730.

Lozier, M. S. (2010), Deconstructing the conveyor belt, *Science*, *328*, 1507–11, doi: 10.1126/science.1189250.

Lozier, M. S. (2012), Overturning in the North Atlantic, *Ann. Rev. Mar. Sci.*, *4*, 291–315, doi:10.1146/annurev-marine-120710-100740.

McCarthy, G. D., D. A. Smeed, W. E. Johns, E. Frajka-Williams, B. I. Moat, D. Rayner, M. O. Baringer, C. S. Meinen, and H. L. Bryden (2015), Measuring the Atlantic meridional overturning circulation at 26°N, *Prog. Oceanogr.*, *130*, 91–111, doi: 10.1016/j.pocean.2014.10.006.

Mielke, C., E. Frajka-Williams, and J. Baehr (2013), Observed and simulated variability of the AMOC at 26°N and 41°N, *Geophys. Res. Lett.*, *40*, 1159–1164, doi: 10.1002/grl.50233.

Roberts, C. D., L. Jackson, and D. McNeall (2014), Is the 2004–2012 reduction of the Atlantic meridional overturning circulation significant?, *Geophys. Res. Lett.*, *41*, 3204–3210, doi:10.1002/2014GL059473.

Send, U., M. Lankhorst, and T. Kanzow (2011), Observation of decadal change in the Atlantic meridional overturning circulation using 10 years of continuous transport data, *Geophys. Res. Lett.*, p. L24606, doi:10.1029/2011GL049801.

Sinha, B., D. A. Smeed, G. McCarthy, B. I. Moat, S. A. Josey, J. J.-M. Hirschi, E. Frajka-Williams, A. T. Blaker, D. Rayner, and G. Madec (2018), The accuracy of estimates of the overturning circulation from basin wide mooring arrays, *Prog. Oceanogr.*, *160*, 101–123, doi:https://doi.org/10.1016/j.pocean.2017.12.001.

Smeed, D. A., G. McCarthy, S. A. Cunningham, E. Frajka-Williams, D. Rayner, W. E. Johns, C. S. Meinen, M. O. Baringer, B. I. Moat, A. Duchez, and H. L. Bryden (2014), Observed decline of the Atlantic meridional overturning circulation 2004 to 2012, *Ocean Sci.*, *10*, 29–38, doi:10.5194/os-10-29-2014.

Srokosz, M. A., and H. L. Bryden (2015), Observing the Atlantic meridional overturning circulation yields a decade of inevitable surprises, *Science*, *348*, 1255,575, doi:10.1126/science.1255575.

Sveshnikov, A. (1968), *Problems in Probability Theory, Mathematical Statistics and Theory of Random Functions*, 481 pp., W.B Saunders Company.

Talley, L. D., G. L. Pickard, W. J. Emery, and J. H. Swift (2011), *Descriptive Physical Oceanography: An Introduction*, 560 pp., Elsevier, Boston.

Toole, J. M., R. G. Curry, T. M. Joyce, M. McCartney, and B. Peña-Molino (2011), Transport of the North Atlantic deep western boundary current about 39°N, 70°W: 2004–2008, *Deep-Sea Res. Pt. II*, *38*, 1768–1780, doi:10.1016/j.dsr2.2010.10.058.

van Sebille, E., M. O. Baringer, W. E. Johns, C. S. Meinen, L. M. Beal, M. F. de Jong, and H. M. van Aken (2011), Propagation pathways of classical Labrader Sea water from its source region to 26°N, *J. Geophys. Res.-Oceans*, *116*, C12,027, doi:10.1029/2011JC007171.

Watts, D. R., and H. Kontoyiannis (1990), Deep-ocean bottom pressure measurement: Drift removal and performance, *J. Atmos. Ocean. Tech.*, *7*, 296–306, doi:10.1175/1520-0426(1990)007<0296:DOBPMD>2.0.CO;2.

Willis, J. K., and L.-L. Fu (2008), Combining altimeter and subsurface float data to estimate the time-averaged circulation in the upper ocean, *J. Geophys. Res.-Oceans*, *113*, C12,017, doi:10.1029/2007JC004690.

Zhang, R. (2010), Latitudinal dependence of Atlantic meridional overturning circulation variations, *Geophys. Res. Lett.*, *37*, L16,703, doi:10.1029/2010GL044474.